AOD-dry $PM_{2.5}$ Relationship with Consideration of Aerosol Type and Hygroscopicity

Kuo-En Chang[1,2], Ta-Chih Hsiao[1,2†], Stephen M. Griffith[3], Yu-Ting Chen[1], Tang-Huang Lin[4], Si-Chee Tsay[5], Hung-Yi Yeh[4], Chian-Yi Liu[2] and Yen-Wei Kuo[4]

[1]Graduate Institute of Environmental Engineering, National Taiwan University, Taipei, Taiwan

[2]Research Centre for Environmental Changes, Academia Sinica, Taipei, Taiwan

[3]Department of Atmospheric Sciences, National Central University, Taoyuan, Taiwan

[4]Center for Space and Remote Sensing Research, National Central University, Taoyuan, Taiwan

[5] NASA Goddard Space Flight Center, Greenbelt, MD, USA

Corresponding author: Ta-Chih Hsiao (tchsiao@ntu.edu.tw)

Key Points:

- A linear relationship, with dependence on aerosol type, hygroscopicity, and boundary layer height, between AOD and dry-PM is derived
- Normalized Gradient Aerosol Index (NGAI) is proposed to differentiate aerosol types and improve surface dry-$PM_{2.5}$ estimations
- The optical hygroscopic growth factor can be estimated by RH-segregated AOD-$PM_{2.5}$ regressions

Abstract

Aerosol type plays a critical role in the relationship between aerosol optical depth (AOD) and particulate matter (PM) mass concentration. Here, we present a mathematical formulation of how $PM_{2.5}$ is related to AOD; when simplified to a linear equation, it reveals a functional dependence of the slope on aerosol type, hygroscopic growth, and boundary layer height, while the influence of the vertical aerosol profile is embedded in the intercept. We further employed a daily averaged AERONET measurement training dataset to develop a Normalized Gradient Aerosol Index (NGAI) for classifying sub-aerosol-types: mineral dust (MD), urban-industrial pollution (U/I) and biomass burning (BB). By distinguishing the aerosol subtypes beforehand, the derived AOD-$PM_{2.5}$ linear regressions were significantly improved, demonstrating that NGAI can exploit the difference in aerosol hygroscopicity and improve the surface dry $PM_{2.5}$ estimations. In addition, the hygroscopic growth factor, f(RH), can be estimated based on the slope (β_1) of the AOD-$PM_{2.5}$ expression.

Keywords: $PM_{2.5}$; Aerosol optical depth; Hygroscopicity; Aerosol type; NGAI

Plain Language Summary

Satellite observations provide an alternative way to depict the spatial distribution surface $PM_{2.5}$. This study derived a mathematical relationship between satellite column aerosol optical depth (AOD) and ground level-dry $PM_{2.5}$, revealing the importance of aerosol type, hygroscopic growth, and boundary layer height. Furthermore, based on the co-variation of AE and AOD resulting from particle growth and photochemical aging, the new aerosol index is proposed to differentiate urban-industrial pollution and biomass burning and improve the accuracy of surface dry-$PM_{2.5}$ estimations. Specifically, the hygroscopic growth factor can also be retrieved based on the AOD-$PM_{2.5}$ relationship.

1 Introduction

In the past decades, fine particulate matter ($PM_{2.5}$), defined as aerosols with an aerodynamic diameter of less than 2.5 μm, has attracted public attention due to its adverse effects on both human health and the environment (Sancini et al., 2014). Ground-level monitoring networks worldwide characterize $PM_{2.5}$ dry-mass concentrations as a metric for air quality assessments and epidemiological studies (Boldo et al., 2011; Kloog et al., 2011; Liang et al., 2016). However, PM concentrations are highly variable on a spatiotemporal scale and not adequately covered by current monitoring networks. To supplement and extend data coverage, satellite remote sensing provides an alternative method to monitor PM on a global scale (Chu et al., 2003; Wang & Christopher, 2003; Liu et al., 2007; Kaskaoutis et al., 2007; You et al., 2016; Lin et al., 2020; Stowell et al., 2020).

One of the most relevant satellite products, the aerosol optical depth (AOD), has been widely used to estimate surface dry-$PM_{2.5}$. Essentially, AOD is an integration of the ambient extinction coefficient due to aerosols. However, satellite AOD retrievals are only applicable for cloud-free conditions. Moreover, there is an inherent mismatch between spatially averaged satellite AOD at a single time point and temporally averaged near-surface $PM_{2.5}$ at a single spatial point. Another issue is the variation in the contribution of $PM_{2.5}$ to the total PM concentration and thus total AOD; this variability is often associated with hygroscopic and coagulation growth of aged fine particles leading to changes in particle size and the granulometric fraction (Cheng et al., 2015). Therefore, the AOD-$PM_{2.5}$ relationship should be a

complicated function of aerosol type, extinction and hygroscopicity, and the vertical atmospheric structure (Tsai et al., 2011; Chu et al., 2013; Lin et al., 2015; Brock et al., 2016). The complexities of the AOD-PM relationship have also been recently summarized, among others, by Jin et al. (2020) and deSouza et al. (2020).

Many studies have focused on the regional relationships of satellite AOD and ground $PM_{2.5}$. Due to the uncertainties associated with satellite AOD retrievals, these studies (e.g., aerosol type classification and AOD-$PM_{2.5}$ relationship investigations) often incorporate ground truth measurements. The globally distributed AERONET (Aerosol Robotic Network), a sun-photometer network, provides near-real-time, multi-spectral observations of aerosol optical properties as an adequate ground-truthing option (Holben et al., 1998). Classification for major aerosol types, including anthropogenic urban-industrial pollution (U/I), biomass burning (BB), sea salt, and mineral dust (MD) (Bellouin et al., 2005), are routinely performed by using AERONET observations of fine-mode fraction (FMF) and Ångström exponent (AE), which is inversely related to average particle radius. However, since U/I and BB aerosols have similar FMFs and are therefore challenging to differentiate, a two-dimensional clustering analysis is often applied to better distinguish U/I and BB aerosols. Also, spectral curvature information has been used for partitioning fine/coarse mode aerosols (O'Neill et al., 2003), where Hansell et al. (2014) demonstrated that the spectral derivative could be used to resolve distinctions in aerosol properties, implying a use for also classifying aerosol types.

In this study, Normalized Gradient Aerosol Index (NGAI), also known as Normalized Derivative Aerosol Index (NDAI) proposed by Lin et al. (2016), is elaborated on further and applied to distinguish aerosol types before analyzing the AOD-$PM_{2.5}$ relationship. The method used in the study is trained by AERONET daily averages for understanding the practicality of daily averages in the sub-aerosol-type classification. Finally, the influence of hygroscopic growth on specific aerosol types is quantified, thus clarifying the AOD-$PM_{2.5}$ relationship and emphasizing the reliability of NGAI.

2 Materials and Methods

AOD, a dimensionless integral (Eqn. 1) of extinction coefficient from the surface to the top-of-atmosphere (TOA), is measured by ground-based sun photometers through transmitted radiance or retrieved through reflected radiance by satellite imaging sensors:

$$AOD = (\lambda) = \int_0^{TOA} \rho(z)\sigma^{ext}(z,\lambda)dz \quad (1)$$

where $\tau(\lambda)$ is AOD at wavelength λ; $\rho(z)$ is PM mass concentration at altitude z ($\mu g/m^3$); $\sigma^{ext}(z,\lambda)$ is aerosol mass extinction efficiency per unit mass ($m^2/\mu g$). To eliminate the inherent mismatch between satellite AOD and surface PM data, this study used collocated ground-based sun photometers to investigate the AOD-$PM_{2.5}$ relationship. It was generally assumed that aerosols are confined and well-mixed within the planetary boundary layer (PBL) (*i.e.*, ρ and σ^{ext} are constant over z). Nevertheless, the actual aerosol extinction coefficient is frequently not zero above the top of PBL and decreases with height. For improving surface $PM_{2.5}$ estimations, the aerosol vertical profile from the top of the PBL was revised by an additional exponential decay in Eqn. 2 and integrated into Eqn. 3 (Tsai et al., 2011; Chu et al., 2013).

$$AOD = \int_0^{PBLH} \rho\sigma^{ext} dz + \int_{PBLH}^{TOA} \rho\sigma^{ext} e^{-\frac{z-PBLH}{H}} dz \quad (2)$$

$$AOD = \sigma^{ext}(PBLH + H) \quad (3)$$

where the characteristic height (H) is the vertical distance that the aerosol extinction coefficient decreases to 1/e of that at the top of PBL (PBLH). However, as revealed by comprehensive measurements via unmanned aerial vehicle (UAV), lidar, and radiosonde, $\rho\sigma^{ext}$ is not a constant even within the PBL (Tian et al., 2017). As a result, Lin et al. (2020) developed a log-normal model, and Li et al. (2016) applied an aerosol bottom isolation factor (as a function of PBLH) to account for the total aerosol vertical profile. In this study, the total aerosol vertical profile is expressed by an arbitrary g function. Eqn. 3 can be rewritten as Eqn. 4 and rearranged as Eqn. 5 to estimate the surface $PM_{2.5}$ concentration:

$$AOD = \sigma^{ext} PBLH - \int_0^{PBLH} \big(\rho\sigma^{ext} - g(z)\big) dz + q \cdot \rho\sigma^{ext} H \quad (4)$$

$$PM_{2.5} \approx \rho = \frac{1}{\sigma_{dry}^{ext} f(RH)(PBLH + aH)} \times \mathrm{AOD} + \frac{\int_0^{PBLH} \big(\rho - g(z)\big) dz}{(PBLH + q \cdot H)}$$

$$= \beta_1 \times \mathrm{AOD} + \beta_0 \quad (5)$$

As shown in the derivation, the surface dry-$PM_{2.5}$ can be estimated by a simple linear function of AOD. For hygroscopic aerosols (*e.g.*, sulfate- and nitrate-dominant), both particle size and extinction efficiency change in a non-linear behavior as the relative humidity (RH) increases. Therefore, $f(RH)$ is included in Eqn. 5 to correct for the influence of hygroscopic growth ($\sigma_{dry}^{ext} f(RH) = \sigma^{ext}$) and is specifically embedded in the slope, β_1, of the AOD-$PM_{2.5}$ regression, which is impacted by PBLH; the influence of vertical aerosol profiles in the PBL is also buried in the intercept, β_0. Through inspecting β_1 and assuming the $f(RH)$ equal to 1.0 at $RH \leq 50\%$, f(RH) can be deduced by taking the ratio of β_1. This idea for estimating f(RH) is proposed and tested for the first time in this study.

2.1 Normalized Gradient Aerosol Index (NGAI)

Atmospheric aerosols are generally classified according to their radiation absorptivity and size (Giles et al., 2012). AE (α), a widely-used indicator for the aerosol type is defined as a function of the spectral wavelength:

$$\alpha(\lambda_1, \lambda_2) = -\frac{\ln(\tau(\lambda_2)/\tau(\lambda_1))}{\ln(\lambda_2/\lambda_1)} \quad (6)$$

The dependency of AE on wavelength is mainly a result of the particle size distribution (PSD) and secondarily due to refractive indices (Eck et al., 1999, 2005; Gobbi et al., 2007; O'Neill et al., 2001). AE is sensitive to effective radius/diameter, known as surface mean diameter (Sauter mean diameter), particularly at < 0.25 μm (Schuster et al., 2006), and is often used as a qualitative indicator of the aerosol particle size. Based on the relative cluster location in an AOD-AE diagram, dust and non-dust aerosols can be distinguished. Nevertheless, Kang et al. (2016) found that the contributions of the more fine-mode aerosols, such as U/I and BB type aerosols, are not necessarily changing significantly with AE. These two types are generally overlapped in the fine-mode region, while they behave differently during hygroscopic growth (Eck et al., 2005; Giles et al., 2012; Kumar et al., 2018; Lee et al., 2010).

The derivative of AE (spectral curvature of AOD) with respect to $\ln \lambda$ has been further proposed to indicate the relative influence of fine/accumulation mode versus coarse mode (Eck et al., 1999, 2005), distinguish aerosol growth from cloud contamination, and observe aerosol humidification (Basart et al., 2009; Che et al., 2015). However, as shown in the two-dimensional AOD-AE clustering analysis, AE is a function of not only wavelength but also AOD. The derivative of AE to AOD could reveal the particle growth dynamics as well as photochemical aging during deteriorating situations. Therefore, an index based on the derivative of $\delta(\lambda_1, \lambda_2)$ with respect to AOD (so-called the Normalized Gradient Aerosol Index, NGAI) has been proposed by Lin et al. (2016) and applied in multiple studies (Lin et al., 2016; Owili et al., 2017). In this study, the concepts of "slope" (δ, changes in AOD with wavelength under linear scale) and "normalization" (changes in slope over changes in AOD) are presented:

$$\delta(\lambda_1, \lambda_2) = -\frac{\tau(\lambda_2) - \tau(\lambda_1)}{\lambda_2 - \lambda_1}$$

$$NGAI = -\frac{d(\delta(\lambda_1, \lambda_2))}{d\tau(\lambda_3)} \quad (7)$$

Training by the AERONET data during event periods (Dataset I), the NGAI threshold is used to distinguish and sub-classify aerosol types previously indistinguishable by AE (i.e., U/I and BB). Furthermore, using different wavelength pairs for NGAI could provide additional information about the size distribution and fine-mode aerosol fraction.

2.2 Ground-based measurements

AERONET is a network of ground-based sun photometers providing a global, long-term dataset of total columnar AOD at standard aerosol wavelengths of 0.340, 0.380, 0.440, 0.500, 0.675, 870, 1.020, and 1.640 μm (Holben et al., 1998; Giles et al., 2019). A sun photometer measures the attenuation of direct solar radiation in the atmosphere; the data is used as a ground truth. Two datasets were employed in this study. Dataset I was for aerosol type classification (Level 2.0 daily averages used). The primary consideration for choosing AERONET sites for Dataset I are (1) the likelihood of a single dominant aerosol type at the site and (2) the temporal completeness of data during the study periods. AERONET level 2.0 daily averages were used in this study, and an AOD threshold of 0.4, suggested in other studies for event cases (Hsu et al., 2006; Ge et al., 2010; M. Kim et al., 2016), was used. Dataset II sites were selected for establishing the AOD-$PM_{2.5}$ relationship (Level 2.0 all points used, 10~15 minutes resolution). AERONET data were obtained from the AERONET website (http://aeronet.gsfc.nasa.gov) from

1997 to 2017. $PM_{2.5}$ mass concentration data were downloaded from the Centre for Environment Monitoring of Vietnam (http://www.cem.gov.vn/), Air Quality and Noise Management Bureau, Pollution Control Department, Thailand (http://www.air4thai.com/webV2/index.php), and Beijing Municipal Ecological and Environmental Monitoring Center (http://www.bjmemc.com.cn/; https://quotsoft.net/air/). $PM_{2.5}$ concentrations were measured by either tapered element oscillating microbalance (TEOM) or beta attenuation monitor (BAM). Location and detailed information of the ground-based measurement data are listed in Table S1.

3 Result and Discussion

3.1 Optical characteristics of aerosol type

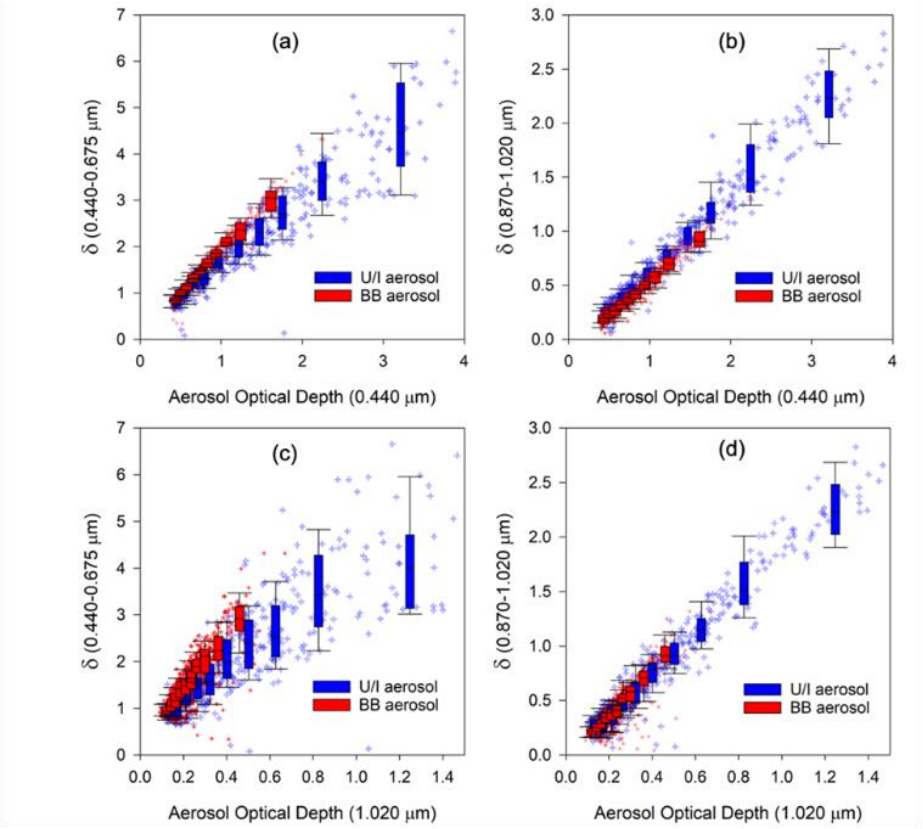

Figure 1. The behavior of δ versus AOD at different paired wavelengths. Panel (a, c) and panel (b, d) are the shorter and longer wavelength pairs to the shortest and longest AOD wavelength, respectively. (c) shows the visual difference in AOD pair with increasing AOD.

In this study, NGAI, the derivative of δ with respect to AOD, was first trained using AERONET daily averages from Dataset I and applied for the aerosol type classification. The NGAIs were calculated based on δ pairs of 0.44-0.67, 0.67-0.87, and 0.87-1.02 μm with respect to AOD wavelengths of 0.44, 0.67, 0.87, and 1.02 nm. As seen in Fig. 1, the distinguishable difference in NGAI between BB and U/I aerosols can be ascribed to the different rates of change in their physicochemical properties (full results for AE and δ variations are shown in Fig. S1 and Fig. S2). As concluded by Kaskaoutis et al. (2006), the co-variation of AE and AOD is the result of both particle growth (due to hygroscopicity, condensation, and coagulation) and

photochemical aging. Thus, NGAI reflects the evolution of PSD and chemical composition as AOD increases, implying the rate at which the aerosol physicochemical properties change during a deteriorating situation. Moreover, the δ behaviors of U/I and BB aerosols are more distinguishable in the short-wavelength pairs compared to the long-wavelength pairs. Thus, NGAI thresholds between U/I and BB aerosols were obtained by an unsupervised K-means clustering algorithm from Fig. 1(a) and Fig. 1(c). The value was -1.71 for NGAI(0.44-0.67, 0.44) with an accuracy of 72.5% (91.0% for BB; 50.7% for U/I), whereas the value for NGAI(0.44-0.67, 1.02) was -6.04 with an accuracy of 75.6% (77.8% for BB; 73.1% for U/I). Notably, the difference between BB and U/I was enhanced for the AOD with a longer wavelength. Kaskaoutis et al. (2006) reported that the co-variation between AE and AOD at shorter wavelengths was more sensitive to fine-mode particle size, while those at longer wavelengths were more sensitive to fine-mode volume fraction. Although the wavelength pairs used in this study differed from those mentioned in Kaskaoutis et al. (2006), the observed behavior still concurs with the findings. The probability distributions of AE and NGAI revealed the wavelength effects as mentioned above (Figure 2). The combination of shorter-pair δ (AOD0.44-0.67) and longer-wavelength AOD (AOD1.02) combined the influences from fine-mode particle size and volume fraction, intensifying the difference.

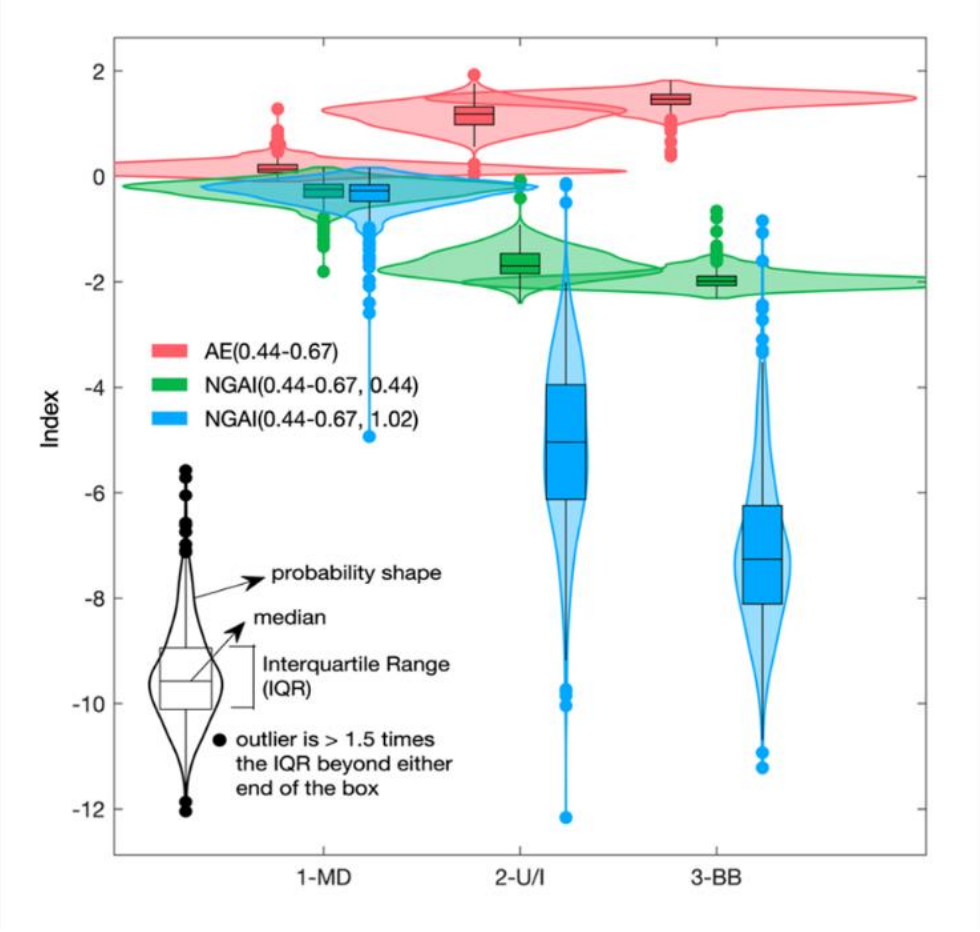

Figure 2. Box-and-violin plots of AE and NGAI for MD, U/I, and BB aerosols include median lines, boxes between 25 and 75 percentiles, and probability distribution shapes (The enclosed area is the same for all).

3.2 AOD-$PM_{2.5}$ relationship

The impact of the NGAI-based aerosol type classification, derived above, on the relationship between AOD and groud $PM_{2.5}$ concentrations in Dataset II was then analyzed. Root Mean Square Error (RMSE) values were determined from the deviations of measured vs. predicted values from AOD-$PM_{2.5}$ regressions. Without NGAI classification, a moderate coefficient of determination ($R^2 = 0.45$) with an RMSE of around 60 μg/m^3 was found in Beijing during the period influenced by dust storms (Figure S3a). For urban areas, a much better correlation ($R^2 = 0.65$) and RMSE (~31 μg/m^3) were observed (Figure S3b). For Chiang Mai, where BB was expected to be the dominant aerosol type, the best correlation ($R^2 = 0.74$) with the lowest RMSE of 10.5 μg/m^3 was observed (Figure S3c). The decreasing slopes and increasing R^2 for expected U/I-dominant and BB-dominant cases suggest a consistent aerosol type with high FMF. Thus, aerosol classification by NGAI, rather than classification simply through location and time, improved the AOD-$PM_{2.5}$ relationship. As seen in Figure S3d, RMSE was reduced from ~60 to ~40 μg/m^3, and R^2 increased to 0.81 for the MD aerosol type, despite Zheng et al. (2017) concluding that coarse non-absorbing aerosols would induce the lowest correlation between AOD and $PM_{2.5}$. To note, only 6% of the Beijing data (18/262) in Dataset II qualified as MD aerosol type by NGAI, suggesting Beijing may not be a good study area for MD aerosols. For the U/I and BB datasets, comparing the pre- and post-NGAI classification data (Fig. S3b, c vs. Fig. S3e, f), the correlations and RMSE were not significantly improved because a single aerosol type already dominated the data sets. The U/I Dataset exhibited the lowest AOD to $PM_{2.5}$ correlation, which may be due to the influences of complex hygroscopic behavior on aerosol optical properties. Nevertheless, after NGAI classification, the AOD-$PM_{2.5}$ regression intercept decreased for all aerosol types, particularly MD and BB cases.

To further elucidate the AOD-$PM_{2.5}$ relationship, the hygroscopic growth factor, *f*(RH), was quantified. However, since the aerosol hygroscopicity varies with chemical compositions, applying *f*(RH) for all types of aerosols could cause over-correction. U/I aerosol composition is typically dominated by the hygroscopic components, such as sulfate and nitrate, while fresh BB aerosols are more hydrophobic and expected to have a smaller *f*(RH). The lesser degree of sensitivity of BB aerosol to RH was evident from the relatively unchanging slope (β_1) and intercept (β_0) of the AOD-$PM_{2.5}$ relationship in Chiang Mai up to RH ~ 80% (Table 1). On the other hand, β_1 decreased and β_0 increased with increasing RH in U/I-dominant conditions. This finding further demonstrates the feasibility of NGAI and stresses the importance of deriving *f*(RH) for each NGAI sub-classified aerosol type. Jung et al. (2021) parameterized the size dependency of *f*(RH) for log-normal distributed aerosols by PSD modeling and applied a simple quadratic function for *f*(RH). Based on Eqn. 5, β_1 is inversely proportional to *f*(RH). Therefore, normalized $1/\beta_1$ values ($\beta_1(RH < 50\%)/\beta_1(RH)$) of U/I aerosols in this study were empirically fitted with respect to the corresponding RH levels (Figure S4a).

$$f(RH) = \frac{\beta_1(RH < 50\%)}{\beta_1(RH)} = 0.612(1 - RH)^{-0.714}, for\ RH > 50\% \quad (8)$$

Our results show a $f(RH \geq 80\%)$ ~2.57 for U/I-dominated aerosols, consistent with earlier publications (Kotchenruther et al., 1999; J. Kim et al., 2006; X. Liu et al., 2008). Furthermore, β_0 values of U/I-dominant conditions were larger than of BB-dominant conditions, which may result from a lower PBLH or inhomogeneous condition for U/I aerosols (i.e., the accumulation of PM near the surface leading to a steep decrease of PM2.5 from the surface to the top of the PBLH; q in Eqn. 5). U/I aerosols are emitted from the surface and tend to accumulate there, while BB aerosols are carried to the upper atmosphere by thermal convection, likely causing such differences in β_0. Thus, the ability of NGAI classification to distinguish U/I and BB aerosols is further supported by segregating the data based on RH levels before regressing the AOD-$PM_{2.5}$ data.

Table 1. AOD-$PM_{2.5}$ aerosol type regression models [a] separated by RH level

Aerosol type	RH (%)	N	β_0	β_1	R^2	RMSE	p-value	$f(RH)$
U/I	≤50 [b]	14	1.90	65.11	0.48	5.02	<0.01	1.00
	50–60	33	12.21	59.56	0.72	23.00	<0.01	1.09
	60–70	43	21.35	57.57	0.76	22.53	<0.01	1.13
	70–80	61	28.40	37.58	0.49	32.13	<0.01	1.73
	≥80	34	34.06	25.30	0.46	23.66	<0.01	2.57
BB	50–60	47	4.15	53.37	0.73	9.47	<0.01	1.00
	60–70	38	4.07	49.57	0.74	12.18	<0.01	1.07
	70–80[c]	39	16.93	26.45	0.35	10.74	<0.01	--
	≥60	95	5.09	45.43	0.76	10.76	<0.01	1.17
	≥80	22	7.82	36.37	0.92	2.19	<0.01	1.47

[a] $PM_{2.5} = \beta_1 \times AOD + \beta_0$

[b] a few points at RH < 50%

[c] low R^2 value

4 Conclusions

A mathematical framework for (i) a unique aerosol type classification index, NGAI, and (ii) an accounting of the vertical atmospheric structural parameters embedded in the AOD-$PM_{2.5}$ relationship were presented in this study. NGAI was established based on the co-variation of AE and AOD resulting from particle growth (due to hygroscopicity, condensation, and coagulation) and photochemical aging. It was then used to distinguish and sub-classify aerosol types (i.e., U/I and BB) previously indistinguishable by two-dimensional AOD-AE clustering analysis. After NGAI classification, larger β_0 values in the AOD-$PM_{2.5}$ regression were generally found for U/I aerosols, which may have been due to lower PBLH and more significant vertical heterogeneity than areas dominated by BB aerosols. In addition, β_1 values were applied to estimate the optical

hygroscopic growth factor, *f*(RH), for different aerosol types. To validate the proposed scheme, AOD and PM data for mixed aerosol types in Beijing were tested. After applying NGAI classification and RH correction, the R^2 value increased from 0.65 to 0.78, and RMSE was reduced (Figure S4b). Most of the improvement was associated with cases of high AOD but low PM, again suggesting high AOD can be caused by hygroscopic aerosol growth. Our results showed that the estimation of dry $PM_{2.5}$ could be improved with the NGAI classification of aerosol type. In the future, the proposed approach can be applied in satellite AOD products for estimating surface dry-$PM_{2.5}$ concentrations.

Conflict of Interest

The authors declare no conflicts of interest relevant to this study.

Data Availability Statement

AERONET data were obtained from the AERONET website (http://aeronet.gsfc.nasa.gov) from 1997 to 2017. $PM_{2.5}$ mass concentration data were downloaded from the Centre for Environment Monitoring of Vietnam (http://www.cem.gov.vn/), Air Quality and Noise Management Bureau, Pollution Control Department, Thailand (http://www.air4thai.com/webV2/index.php), and Beijing Municipal Ecological and Environmental Monitoring Center (http://www.bjmemc.com.cn/; https://quotsoft.net/air/).

Acknowledgments

This work was financially supported by the National Taiwan University (NTU) within the framework of the Higher Education Sprout Project by the Ministry of Education (MOE) in Taiwan (Grant No. 109L4000), and the Research Centre for Environmental Changes (RCEC), Academia Sinica in Taiwan (Grant No. AS-GC-110-01).

References

Basart, S., Pérez, C., Cuevas, E., Baldasano, J. M., & Gobbi, G. P. (2009). Aerosol characterization in Northern Africa, Northeastern Atlantic, Mediterranean Basin and Middle East from direct-sun AERONET observations. *Atmos. Chem. Phys*, *9, (21)*, 8265–8282.

Bellouin, N., Boucher, O., Haywood, J., & Reddy, M. S. (2005). Global estimate of aerosol direct radiative forcing from satellite measurements. *Nature, 438, (7071)*, 1138–1141.

Boldo, E., Linares, C., Lumbreras, J., Borge, R., Narros, A., García-Pérez, J., et al. (2011). Health impact assessment of a reduction in ambient PM2.5 levels in Spain. *Environment International*, *37, (2)*, 342–348.

Brock, C. A., Wagner, N. L., Anderson, B. E., Attwood, A. R., Beyersdorf, A., Campuzano-Jost, P., et al. (2016). Aerosol optical properties in the southeastern United States in summer – Part 1: Hygroscopic growth. *Atmos. Chem. Phys*, *16, (8)*, 4987–5007.

Che, H., Zhao, H., Wu, Y., Xia, X., Zhu, J., Dubovik, O., et al. (2015). Application of aerosol optical properties to estimate aerosol type from ground-based remote sensing observation at urban area of northeastern China. *Journal of Atmospheric and Solar-Terrestrial Physics*, *132*, 37–47.

316 Cheng, T., Xu, C., Duan, J., Wang, Y., Leng, C., Tao, J., et al. (2015). Seasonal variation and
317 difference of aerosol optical properties in columnar and surface atmospheres over
318 Shanghai. *Atmospheric Environment*, *123*, 315–326.

319 Chu, D. A., Kaufman, Y. J., Zibordi, G., Chern, J. D., Mao, J., Li, C., & Holben, B. N. (2003).
320 Global monitoring of air pollution over land from the Earth Observing System-Terra
321 Moderate Resolution Imaging Spectroradiometer (MODIS. *Journal of Geophysical*
322 *Research: Atmospheres*, *108*, 21.

323 Chu, D. A., Tsai, T. C., Chen, J. P., Chang, S. C., Jeng, Y. J., Chiang, W. L., & Lin, N. H.
324 (2013). Interpreting aerosol lidar profiles to better estimate surface PM2.5 for columnar
325 AOD measurements. *Atmospheric Environment*, *79*, 172–187.

326 deSouza, P., Kahn, R. A., Limbacher, J. A., Marais, E. A., Duarte, F., & Ratti, C. (2020).
327 Combining low-cost, surface-based aerosol monitors with size-resolved satellite data for
328 air quality applications. *Atmos. Meas. Tech*, *13, (10)*, 5319–5334.

329 Eck, T. F., Holben, B. N., Reid, J. S., Dubovik, O., Smirnov, A., O'Neill, N. T., et al. (1999).
330 Wavelength dependence of the optical depth of biomass burning, urban, and desert dust
331 aerosols. *Journal of Geophysical Research: Atmospheres*, *104, (D24)*, 31333–31349.

332 Eck, T. F., Holben, B. N., Dubovik, O., Smirnov, A., Goloub, P., Chen, H. B., et al. (2005).
333 Columnar aerosol optical properties at AERONET sites in central eastern Asia and
334 aerosol transport to the tropical mid-Pacific. *Journal of Geophysical Research:*
335 *Atmospheres*, *110*, 6.

336 Ge, J. M., Su, J., Ackerman, T. P., Fu, Q., Huang, J. P., & Shi, J. S. (2010). Dust aerosol optical
337 properties retrieval and radiative forcing over northwestern China during the 2008 China-
338 U.S. joint field experiment. *Journal of Geophysical Research: Atmospheres*, *115*, 7.

339 Giles, D. M., Holben, B. N., Eck, T. F., Sinyuk, A., Smirnov, A., Slutsker, I., et al. (2012). An
340 analysis of AERONET aerosol absorption properties and classifications representative of
341 aerosol source regions. *Journal of Geophysical Research: Atmospheres*, *117*(D17).

342 Giles, D. M., Sinyuk, A., Sorokin, M. G., Schafer, J. S., Smirnov, A., Slutsker, I., et al. (2019).
343 Advancements in the Aerosol Robotic Network (AERONET) Version 3 database –
344 automated near-real-time quality control algorithm with improved cloud screening for
345 Sun photometer aerosol optical depth (AOD) measurements. *Atmos. Meas. Tech*, *12, (1*,
346 169–209.

347 Gobbi, G. P., Kaufman, Y. J., Koren, I., & Eck, T. F. (2007). Classification of aerosol properties
348 derived from AERONET direct sun data. *Atmos. Chem. Phys*, *7, (2)*, 453–458.

349 Hansell, R. A., Tsay, S.-C., Pantina, P., Lewis, J. R., Ji, Q., & Herman, J. R. (2014). Spectral
350 derivative analysis of solar spectroradiometric measurements: Theoretical basis. *Journal*
351 *of Geophysical Research: Atmospheres*, *119, (14)*, 8908–8924.

352 Holben, B. N., Eck, T. F., Slutsker, I., Tanré, D., Buis, J. P., Setzer, A., et al. (1998).
353 AERONET—A Federated Instrument Network and Data Archive for Aerosol
354 Characterization. *Remote Sensing of Environment*, *66, (1)*, 1–16.

Hsu, N. C., Tsay, S., King, M. D., & Herman, J. R. (2006). Deep Blue Retrievals of Asian Aerosol Properties During ACE-Asia. *IEEE Transactions on Geoscience and Remote Sensing, 44, (11)*, 3180–3195.

Jin, Q., Crippa, P., & Pryor, S. C. (2020). Spatial characteristics and temporal evolution of the relationship between PM2.5 and aerosol optical depth over the eastern USA during 2003–2017. *Atmospheric Environment, 239*, 117718.

Jung, C. H., Yoon, Y. J., Um, J., Lee, S. S., Han, K. M., Shin, H. J., et al. (2021). Approximated expression of the hygroscopic growth factor for polydispersed aerosols. *Journal of Aerosol Science, 151*, 105670.

Kang, N., Kumar, K. R., Yu, X., & Yin, Y. (2016). Column-integrated aerosol optical properties and direct radiative forcing over the urban-industrial megacity Nanjing in the Yangtze River Delta, China. *Environmental Science and Pollution Research, 23, (17)*, 17532–17552.

Kaskaoutis, D. G., Kambezidis, H. D., Adamopoulos, A. D., & Kassomenos, P. A. (2006). On the characterization of aerosols using the Ångström exponent in the Athens area. *Journal of Atmospheric and Solar-Terrestrial Physics, 68, (18)*, 2147–2163.

Kaskaoutis, D. G., Kambezidis, H. D., Hatzianastassiou, N., Kosmopoulos, P. G., & Badarinath, K. V. S. (2007). Aerosol climatology: dependence of the Angstrom exponent on wavelength over four AERONET sites. *Atmos. Chem. Phys. Discuss*, 7347–7397.

Kim, J., Yoon, S.-C., Jefferson, A., & Kim, S.-W. (2006). Aerosol hygroscopic properties during Asian dust, pollution, and biomass burning episodes at Gosan, Korea in April 2001. *Atmospheric Environment, 40, (8)*, 1550–1560.

Kim, M., Kim, J., Jeong, U., Kim, W., Hong, H., Holben, B., et al. (2016). Aerosol optical properties derived from the DRAGON-NE Asia campaign, and implications for a single-channel algorithm to retrieve aerosol optical depth in spring from Meteorological Imager (MI) on-board the Communication, Ocean, and Meteorological Satellite (COMS. *Atmos. Chem. Phys, 16, (3)*, 1789–1808.

Kloog, I., Koutrakis, P., Coull, B. A., Lee, H. J., & Schwartz, J. (2011). Assessing temporally and spatially resolved PM2.5 exposures for epidemiological studies using satellite aerosol optical depth measurements. *Atmospheric Environment, 45, (35)*, 6267–6275.

Kotchenruther, R. A., Hobbs, P. V., & Hegg, D. A. (1999). Humidification factors for atmospheric aerosols off the mid-Atlantic coast of the United States. *Journal of Geophysical Research: Atmospheres, 104, (D2)*, 2239–2251.

Kumar, K.R., Kang, N., & Yin, Y. (2018). Classification of key aerosol types and their frequency distributions based on satellite remote sensing data at an industrially polluted city in the Yangtze River Delta, China. *International Journal of Climatology, 38, (1)*, 320–336.

Lee, J., Kim, J., Song, C. H., Kim, S. B., Chun, Y., Sohn, B. J., & Holben, B. N. (2010). Characteristics of aerosol types from AERONET sunphotometer measurements. *Atmospheric Environment, 44, (26)*, 3110–3117.

Li, Z., Zhang, Y., Shao, J., Li, B., Hong, J., Liu, D., et al. (2016). Remote sensing of atmospheric particulate mass of dry PM2.5 near the ground: Method validation using ground-based measurements. *Remote Sensing of Environment*, *173*, 59–68.

Liang, X., Li, S., Zhang, S., Huang, H., & Chen, S. X. (2016). PM2.5 data reliability, consistency, and air quality assessment in five Chinese cities. *Journal of Geophysical Research: Atmospheres*, *121*, *(17)*, 10,220-10,236.

Lin, C., Li, Y., Yuan, Z., Lau, A. K. H., Li, C., & Fung, J. C. H. (2015). Using satellite remote sensing data to estimate the high-resolution distribution of ground-level PM2.5. *Remote Sensing of Environment*, *156*, 117–128.

Lin, T. H., Liu, G. R., & Liu, C. Y. (2016). A novel index for atmospheric aerosol type categorization with spectral optical depths from satellite retrieval. *Int. Arch. Photogramm. Remote Sens. Spat. Inf. Sci*, *8*, 277–279.

Lin, T. H., Chang, K. E., Chan, H. P., Hsiao, T. C., Lin, N. H., Chuang, M. T., & Yeh, H. Y. (2020). Potential Approach for Single-Peak Extinction Fitting of Aerosol Profiles Based on In Situ Measurements for the Improvement of Surface PM2.5 Retrieval from Satellite AOD Product. *Remote Sensing*, *12, (13)*, 2174.

Liu, X., Cheng, Y., Zhang, Y., Jung, J., Sugimoto, N., Chang, S.-Y., et al. (2008). Influences of relative humidity and particle chemical composition on aerosol scattering properties during the 2006 PRD campaign. *Atmospheric Environment*, *42, (7)*, 1525–1536.

Liu, Y., Franklin, M., Kahn, R., & Koutrakis, P. (2007). Using aerosol optical thickness to predict ground-level PM2.5 concentrations in the St. Louis area: A comparison between MISR and MODIS. *Remote Sensing of Environment*, *107, (1)*, 33–44.

O'Neill, N. T., Eck, T. F., Holben, B. N., Smirnov, A., Dubovik, O., & Royer, A. (2001). Bimodal size distribution influences on the variation of Angstrom derivatives in spectral and optical depth space. *Journal of Geophysical Research: Atmospheres*, *106, (D9)*, 9787–9806.

O'Neill, N. T., Eck, T. F., Smirnov, A., Holben, B. N., & Thulasiraman, S. (2003). Spectral discrimination of coarse and fine mode optical depth. *Journal of Geophysical Research: Atmospheres*, *108*(D17).

Owili, P. O., Lien, W.-H., Muga, M. A., & Lin, T.-H. (2017). The Associations between Types of Ambient PM2.5 and Under-Five and Maternal Mortality in Africa. *International Journal of Environmental Research and Public Health*, *14, (4)*, 359.

Sancini, G., Farina, F., Battaglia, C., Cifola, I., Mangano, E., Mantecca, P., et al. (2014). Health risk assessment for air pollutants: alterations in lung and cardiac gene expression in mice exposed to Milano winter fine particulate matter (PM2.5). *PloS One*, *9*(10), e109685.

Schuster, G. L., Dubovik, O., & Holben, B. N. (2006). Angstrom exponent and bimodal aerosol size distributions. *Journal of Geophysical Research: Atmospheres*, *111*, 7.

Stowell, J. D., Bi, J., Al-Hamdan, M. Z., Lee, H. J., Lee, S.-M., Freedman, F., et al. (2020). Estimating PM2.5 in Southern California using satellite data: factors that affect model performance. *Environmental Research Letters*, *15, (9)*, 094004.

Tian, P., Cao, X., Zhang, L., Sun, N., Sun, L., Logan, T., et al. (2017). Aerosol vertical distribution and optical properties over China from long-term satellite and ground-based remote sensing. *Atmos. Chem. Phys, 17, (4)*, 2509–2523.

Tsai, T. C., Jeng, Y. J., Chu, D. A., Chen, J. P., & Chang, S. C. (2011). Analysis of the relationship between MODIS aerosol optical depth and particulate matter from 2006 to 2008. *Atmospheric Environment*, *45, (27)*, 4777–4788.

Wang, J., & Christopher, S. A. (2003). Intercomparison between satellite-derived aerosol optical thickness and PM2.5 mass: Implications for air quality studies. *Geophysical Research Letters*, *30*, 21.

You, W., Zang, Z., Zhang, L., Li, Y., Pan, X., & Wang, W. (2016). National-Scale Estimates of Ground-Level PM2.5 Concentration in China Using Geographically Weighted Regression Based on 3 km Resolution MODIS AOD. *Remote Sensing, 8, (3)*, 184.

Zheng, C., Zhao, C., Zhu, Y., Wang, Y., Shi, X., Wu, X., et al. (2017). Analysis of influential factors for the relationship between PM2.5 and AOD in Beijing. *Atmos. Chem. Phys, 17, (21)*, 13473–13489.